International Journal of Microwave and Wireless Technologies

cambridge.org/mrf

Broadband high gain cavity resonator antenna using planar electromagnetic bandgap (EBG) superstrate

Soumik Dey and Sukomal Dey

Department of Electrical Engineering, Indian Institute of Technology Palakkad, Kerala 678557, India

Research Paper

Cite this article: Dey S, Dey S (2023). Broadband high gain cavity resonator antenna using planar electromagnetic bandgap (EBG) superstrate. *International Journal of Microwave and Wireless Technologies* **15**, 90–101. https://doi.org/10.1017/S1759078721001768

Received: 8 September 2021
Revised: 15 December 2021
Accepted: 16 December 2021
First published online: 11 January 2022

Key words:
Antenna array; broadband; electromagnetic bandgap; Fabry–Perot cavity resonator antenna; partially reflecting surface; reactive impedance surface

Author for correspondence:
Sukomal Dey,
E-mail: sukomal.iitpkd@gmail.com

Abstract

This paper presents a broadband miniaturized Fabry–Perot cavity resonator antenna (CRA) made of novel electromagnetic bandgap (EBG) superstrate as partially reflecting surface (PRS) and reactive impedance surface (RIS) backed rectangular patch antenna. To the best of the authors' knowledge, the proposed EBG exhibits the highest stopband bandwidth (BW) with a bandgap existing between 7.37 and 12.4 GHz (50.9%). Frequency-selective property of the EBG is utilized under plane wave incidence to demonstrate it as PRS superstrate in CRA antenna. The cavity is excited with a rectangular microstrip antenna which is made of two dielectric substrates with an additional RIS layer sandwiched between them. The RIS provides wideband impedance matching of the primary feed antenna. A 7×7 array of the EBG superstrate is loaded over the patch antenna having an overall lateral dimension of only 45×45 mm^2 or $1.62\ \lambda_0 \times 1.62\ \lambda_0$ where λ_0 is the free space wavelength at the center frequency of 10.8 GHz. The proposed Fabry–Perot CRA (FP-CRA) achieves gain enhancement of 6.59 dB as compared with the reference antenna and has a 10 dB return loss BW of 23.79% from 10.07 to 12.79 GHz. A prototype of the FP-CRA is fabricated and experimentally tested with single and dual layers of EBG superstrate. Measured results show BWs of 21.5 and 24.8% for the two cases with peak realized gain of 12.05 and 14.3 dBi, respectively. Later a four-element antenna array with corporate feeding is designed as the primary feed of the CRA. The simulation result shows a flat gain of >13 dBi with gain variation <1.2 dB over the impedance BW of 13.2%.

Introduction

Electromagnetic bandgap (EBG) as a periodic 2D element is gaining a lot of interest for passive microwave circuit and antenna design due to their attractive interaction with electromagnetic (EM) waves [1]. EBG is broadly classified as mushroom [2] and uniplanar type [3], which exhibits properties such as surface wave suppression within its frequency bandgap and in-phase reflection for plane wave incidence. EBG is integrated with a planar array for mutual coupling reduction [4] and low profile compact antenna design [5]. In recent years, different miniaturized mushroom [6–8] and uniplanar EBG [9–11] geometries are reported and their applications are presented in detail. EBG acts as frequency-selective surface (FSS) when the backside ground plane is removed [12]. FSS found application as partially reflecting surface (PRS) in cavity resonator antenna (CRA) for directivity enhancement [13]. EBG superstrate-loaded Fabry–Perot cavity resonator antenna (FP-CRA) achieves high gain without complex feeding, but their bandwidth (BW) is limited usually <3%. Modern wireless and satellite communication demands a compact high-gain broadband antenna. Several BW broadening techniques have been reported such as stacking radiating patches, etching U-shaped slot, and parasitic gap coupling [14–16]. Metamaterial-inspired broadband mushroom antenna is proposed by combining high-order modes [17]. Reactive impedance surface (RIS) consists of periodic square patches incorporated between the radiating patch and ground plane for achieving miniaturization and wideband impedance matching [18]. The average gain of the broadband antennas in [14–18] varies between 6 and 8 dBi and suffers from low aperture efficiency and low front-to-back ratio (FTBR). Conventional gain enhancement methods – antenna array, dielectric lenses, back reflector – achieve high gain at the expense of design complexity, power loss in the feed network, large volume, and high cost. On contrary, the FP-CRA presents a simple solution for improving the gain of a microstrip antenna without additional losses in the feed [19–29]. BW of FP-CRA was enhanced using vertical stacking of multilayer PRS [24], using FSS and its complementary geometry [27, 28]. Alternately broadband impedance matching can be achieved by increasing the BW of the reference antenna using air dielectric between the radiating patch and the ground plane, waveguide radiator, and antenna array. This causes large lateral dimension, high sidelobe level (SLL), heavy weight, bulky geometry, and antenna performance is more sensitive to fabrication tolerance. It is challenging to design a broadband

© The Author(s), 2022. Published by Cambridge University Press in association with the European Microwave Association

CAMBRIDGE UNIVERSITY PRESS

high-gain FP-CRA on a small footprint without compromising the overall profile and fabrication difficulties.

In this paper, a novel uniplanar EBG is presented with a property of wide frequency bandgap. FSS characteristic of the proposed EBG is utilized to design a compact broadband high-gain FP-CRA. The radiation pattern of the antenna shows a high FTBR and good co to cross-polarized (XPol) discrimination in both principal planes. The paper is organized as follows: "Design of proposed compact uniplanar EBG" section discusses the geometry of the proposed EBG, its simulation results, and the state-of-the-art performance comparison with earlier reported unit cells. "Fabry–Perot cavity resonator antenna (FP-CRA)" section presents the proposed broadband CRA with EBG as a superstrate and the operating principle of the antenna. Experimental results of the antenna are illustrated in "Experimental results" section followed by a performance comparison of the antenna with previous works. "Antenna array with EBG superstrate" section presents a four-element antenna array-driven FP-CRA and the simulation results of the designed array. Finally, the paper is concluded in "Conclusion" section.

Design of proposed compact uniplanar EBG

Unit-cell geometry

Figure 1(a) shows the layout of the proposed uniplanar EBG which consists of two metal layers separated by a dielectric substrate. The back metal layer acts as a complete perfect electric conductor (PEC) ground plane. The unit-cell geometry is printed on the front side of the substrate and has a 2D periodic configuration. The substrate material is Taconic TLC-32 (relative permittivity $e_r = 3.2$ and loss tangent tan $\delta = 0.003$) having a thickness of 0.79 mm. The proposed unit cell consists of interdigital capacitors (IDC) along the outer edges and a four-arm spiral resonator at the center making it interconnected with corner square patches of length l_i. Fingers of the IDC are folded to adjust the overall capacitance of the structure. Each unit element is connected at the corners with adjacent unit cells. Hence in a full 2D array configuration, surface current in the spiral resonator flows from one unit cell to its adjacent ones and causes an increase in total inductance. The periodicity (P_c) of the proposed EBG is 4.2 mm or 0.13 λ_0, where λ_0 is free space wavelength at the center frequency of the bandgap. The final dimensions of the unit cell are $l_f = 0.$ 98 mm, $l_i = 1.12$ mm, $w = 0.15$ mm, $g = 0.15$ mm.

Dispersion characteristics

EBG is generally characterized by its dispersion diagram which is a graphical representation of phase constant (β) and the wavenumber (k). For EBG, non-linear variation of β (or k) relative to frequency exists due to its lossy nature. EBG assists the propagation of different surface wave modes, each of them having a unique field configuration. The lowest propagation mode is transverse magnetic (TM) with zero cut-off frequency. Periodic geometry of EBG allows the existence of frequency bandgap between two modes. Within the bandgap, EBG suppresses the surface wave propagation. The proposed EBG is simulated in Eigen mode solver of high-frequency structure simulator (HFSS) by imposing periodic boundary conditions. Eigen mode frequencies are determined only over the Brillouin zone triangle consisting of Γ-X-M due to 90° rotational symmetry in the proposed geometry. The dispersion diagram of the proposed EBG is depicted in Fig. 1(b) and the result shows a bandgap from 7.37 to 12.4 GHz (50.9%) between the first two modes. The bandgap covers the entire X-band of the microwave spectrum.

The aforementioned bandgap is further characterized by placing a seven-element 1D EBG array on both sides of a 50 Ω microstrip line as illustrated in Fig. 2(a). The spacing between the transmission line (TL) and the EBG array is 0.15 mm. Capacitive coupling between the proposed EBG and TL interacts with propagating transverse EM wave and opposes the propagation of the wave over specific frequency regions due to EBG's resonance nature. Figure 2(b) shows the transmission coefficient (S_{21}) of the EBG-loaded TL which exhibits two narrow stopbands at the center at 6.75 and 13.15 GHz. An increase in capacitance between the EBG and TL causes a shift of the first stopband frequency at a lower frequency range [9]. The BW of two stopbands with $S_{21}<-3$ dB are over 6.21–6.97 GHz (11.53%) and from 12.76 to 14.1 GHz (9.98%).

EBG as frequency-selective surface

The reflection and transmission coefficients of the proposed EBG are determined for plane wave incidence. The back metal layer of the EBG is removed to allow transmission through the structure. Scattering parameters are obtained from full-wave numerical simulation under Floquet port excitation. The results are compared with the circuit simulation and the measured filter response is obtained using the waveguide measurement technique. Figure 3(a) exhibits the experimental setup for waveguide measurement with FSS placed inside the sample holder. EM wave impinges on the FSS from WR-90 waveguide with an operating range between 8.2 and 12.4 GHz. Two such waveguides act as the source and the receptor of the EM waves. The equivalent circuit of the proposed FSS is modeled as parallel resonant circuit L_p-C_p as shown in Fig. 3(b). The effect of the dielectric substrate is taken into consideration by representing it as a short TL of characteristics impedance $Z_s = Z_0/\sqrt{\varepsilon_r}$and the length h same as the substrate thickness. Here Z_0 is the wave impedance of free space having a value of 120 π or 377 Ω. While the surface current through the spiral resonator at the center contributes to total inductance (L_p), the fringing field between the fingers of IDC attributes to the capacitance (C_p). Numerical and circuit simulations of the proposed FSS are shown in Fig. 3(c) over the frequency sweep of 5–15 GHz. Final values of L_p and C_p are obtained using the curve fitting method in a circuit simulator and the values are 1.56 nH and 0.17 pF. The proposed FSS shows a simulated passband center at 9.32 GHz. The 3 dB transmission BW ($S_{21} > -3$ dB) extends over 7.16–11.61 GHz (47.4%). Inside the X-band frequency range, measured scattering parameters are found consistent with the simulation results except for little discrepancies at the band edges. The discrepancy is caused by an increase in attenuation outside the operating range of the WR-90 waveguide.

To illustrate the angular stability of the proposed FSS, the reflection and transmission coefficients of the FSS are simulated at different incidence angles. The simulated result in Fig. 4 exhibits a stable passband filter response of the FSS up to a high oblique incidence of 60° for both transverse electric (TE) and TM polarizations. The shifts in resonance frequency are <0.86% for TE mode and <4.5% for TM mode. The performance of the proposed EBG is compared with earlier reported unit cells in Table 1. Compared to unit cells in [4, 6–11], the proposed geometry achieves a higher bandgap with comparable unit-cell periodicity and thickness. Moreover relative to mushroom-type EBGs in

https://doi.org/10.1017/S1759078721001768 Published online by Cambridge University Press

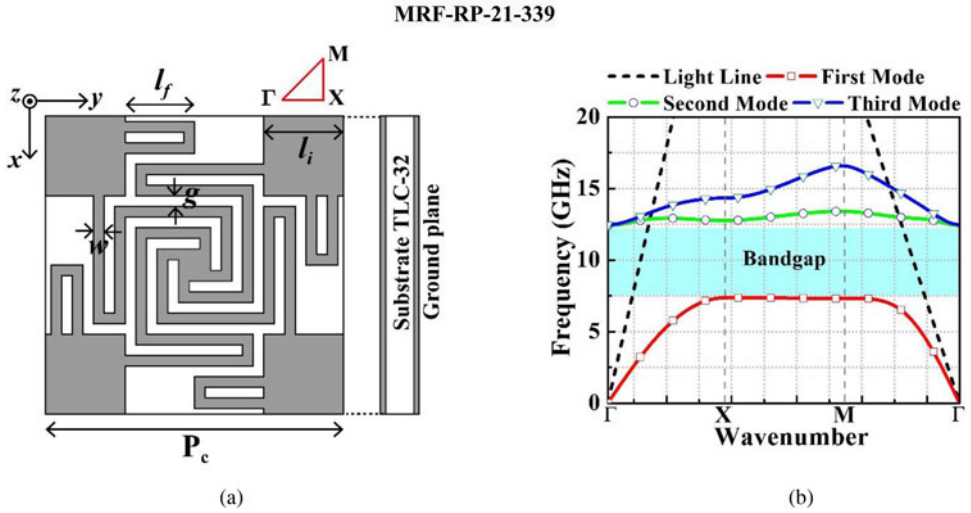


Fig. 1. (a) Geometry of the proposed uniplanar EBG – front and side views; (b) simulated dispersion diagram.

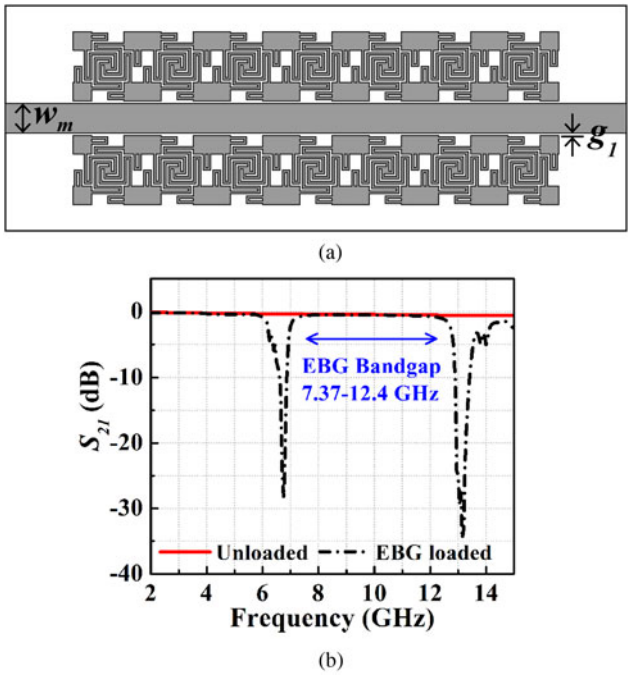


Fig. 2. (a) Schematic diagram of EBG coupled with microstrip line; (b) simulated transmission coefficients of EBG-unloaded and loaded transmission line. Design parameters are: $w_m = 1.9$ mm and $g_1 = 0.15$ mm.

[4, 6–8], the proposed uniplanar configuration has an added advantage of less fabrication complexity due to the absence of metallic via.

Fabry–Perot cavity resonator antenna (FP-CRA)

The FSS characteristic of the proposed EBG is utilized in this paper to design a broadband high-gain CRA. The proposed EBG acts as a PRS superstrate over a broadband microstrip antenna. The primary feed antenna is a RIS-backed radiating patch which is characterized by wideband impedance matching, improved radiation performance, increase in FTBR, and reduced mutual coupling between the radiating patch and the ground plane.

RIS-backed broadband antenna

RIS exhibits in-phase reflection near its resonance for a plane wave incidence [18]. Away from the resonance, the inductive reactance of RIS compensates for the capacitance associated with the electric energy stored in the antenna near-field region. This results in broadband impedance matching and miniaturization of radiating patch dimensions. In the present work, RIS consists of periodic square patches of array size 8×8 on a ground-backed TLC-32 substrate with a height of 0.79 mm. RIS unit cell has periodicity (D_x) 3.27 mm with a square patch length (a) of 2.87 mm. The copper with a thickness (t) of 0.035 mm is used as conducting material. The grounded dielectric substrate is modeled as short-circuited TL, which provides an equivalent inductance according to TL theory. The spacing between the adjacent square patches contributes to capacitance in parallel. The simulated reflection phase of the proposed RIS unit cell and its simulation setup for plane wave incidence are depicted in Fig. 5. The wave is incident along the Z-axis with the perfect magnetic conductor and PEC boundaries are assigned in the YZ and XZ planes, respectively. Figure 5(b) shows that the reflection phase varies from +180° to −180° and it decreases with the increase in frequency. The zero-crossing of the phase occurs at 11.8 GHz. The operating BW of the RIS is 10.36–12.92 GHz (22%) over which the reflection phase varies between +90° and −90°.

Figure 6(a) represents the layout of the rectangular patch antenna with the RIS-backed ground plane. Radiating patch has length (L_p) 5.8 mm, width (W_p) 7.6 mm, and it is printed on Taconic TLC-32 substrate with a height of 0.79 mm. The probe feeding is used to excite the antenna with the probe being located at a distance P_x from the center along the x-axis. Simulation of the proposed patch antenna is performed in HFSS and the results are shown in Figs 7(a) and Figs 7(b). Antenna resonates at 11.1 GHz with a simulated impedance BW of $S_{11} < -10$ dB from 10.31 to 12.76 GHz (21.24%) and having peak realized gain of 6.02 dBi.

https://doi.org/10.1017/S1759078721001768 Published online by Cambridge University Press

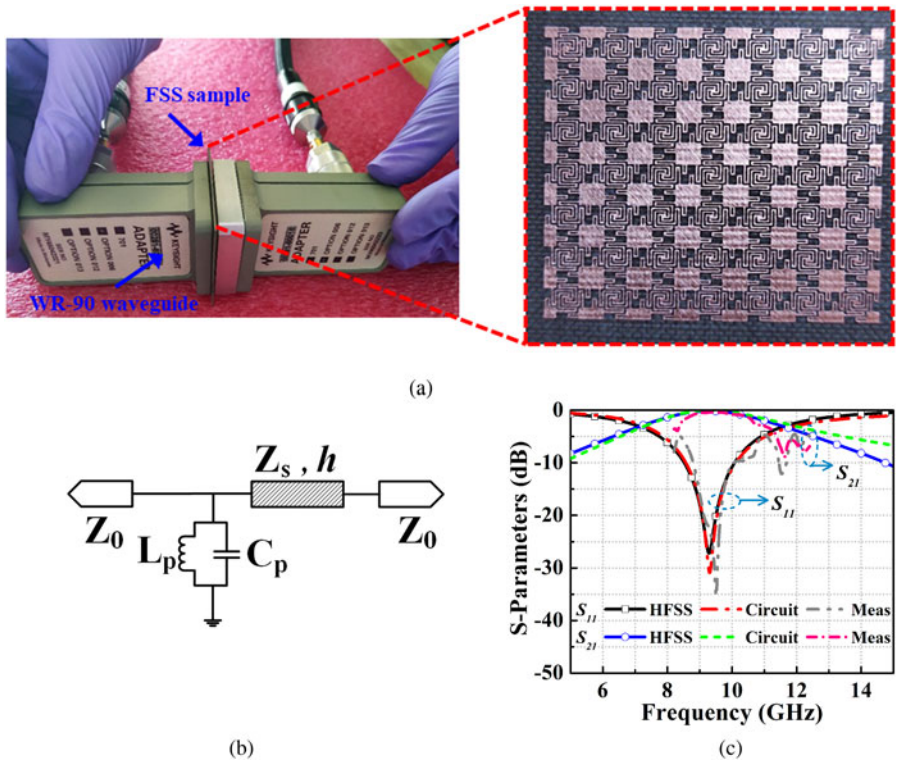


Fig. 3. (a) Waveguide measurement setup for the proposed EBG acting as FSS for plane wave incidence; (b) equivalent circuit model of the FSS; (c) simulated and measured reflection and transmission coefficients.

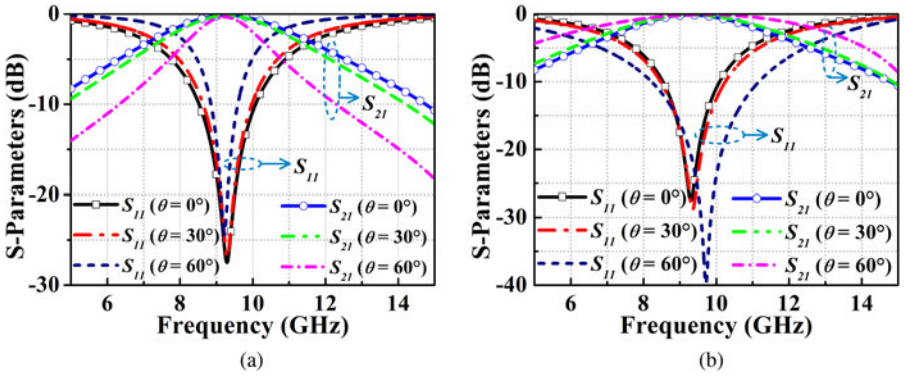


Fig. 4. Simulated reflection and transmission coefficients of the EBG acting as FSS for different incidence angles: (a) TE mode; (b) TM mode.

Table 1. State-of-the-art performance comparison of the proposed uniplanar EBG with previously reported unit cells

Ref.	Center frequency (GHz)	Bandgap	Unit-cell periodicity (λ_0)	Thickness (λ_0)	Type
[4]	5.5	5–6 GHz (18.18%)	0.1	0.029	Mushroom
[6]	5.36	4.79–5.92 GHz (20.2%)	0.08	0.035	Mushroom
[7]	5.63	5.34–5.92 GHz (10.3%)	0.029	0.048	Mushroom
[8]	3.195	3.01–3.38 GHz (11.6%)	0.096	0.016	Mushroom
[9]	6.69	5.48–7.9 GHz (36.17%)	0.096	0.017	Uniplanar
[10]	4.55	4.1–5 GHz (19.78%)	0.109	0.023	Uniplanar
[11]	4.7	3.8–5.6 GHz (38.29%)	0.191	0.01	Uniplanar
Proposed EBG	**9.88**	**7.37–12.4 GHz (50.9%)**	**0.13**	**0.026**	**Uniplanar**

https://doi.org/10.1017/S1759078721001768 Published online by Cambridge University Press

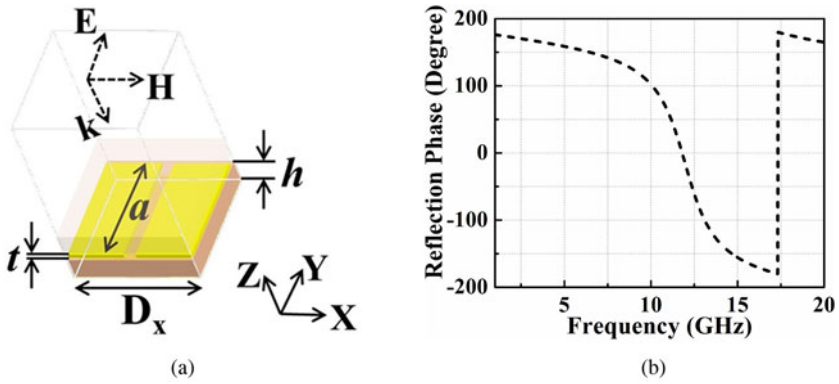


Fig. 5. (a) RIS unit cell with simulation setup for plane wave incidence; (b) simulated reflection phase.

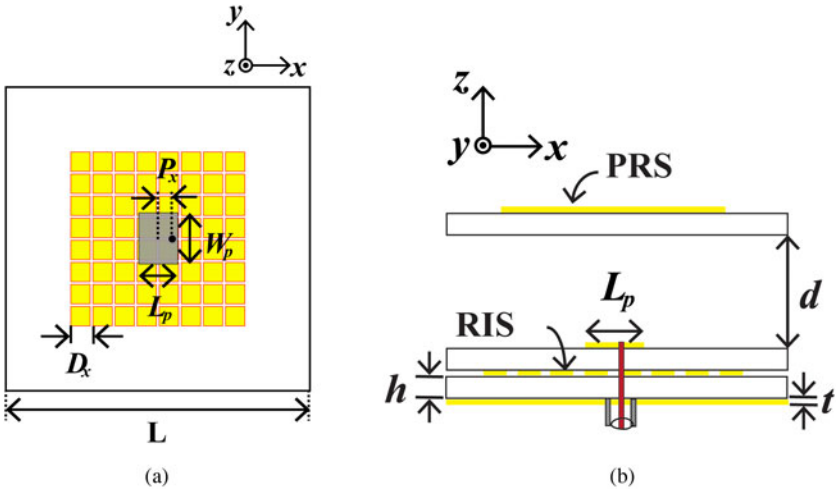


Fig. 6. (a) Schematic of the proposed broadband antenna on RIS; (b) side view of the proposed FP-CRA with EBG as PRS.

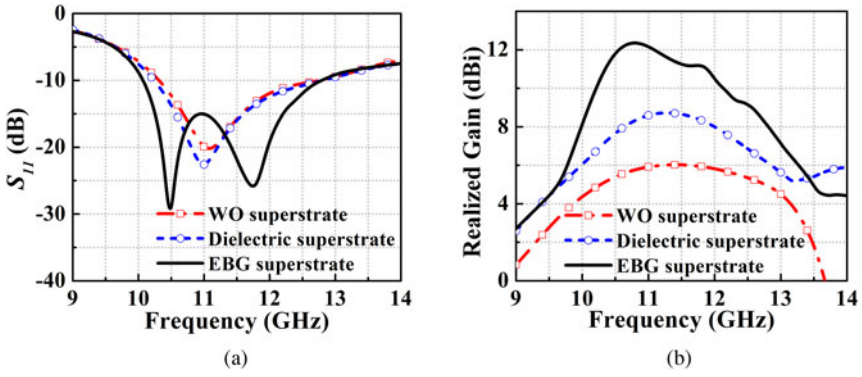


Fig. 7. Simulated (a) reflection coefficient and (b) gain characteristics of the proposed broadband reference antenna and the EBG superstrate-loaded FP-CRA.

Antenna with EBG superstrate

Low directivity of the proposed RIS-backed patch antenna is enhanced by placing an EBG superstrate over the radiator at a distance d from the patch surface as depicted in Fig. 6(b). The ground plane of the antenna and the superstrate layer form the two reflecting surfaces of the Fabry–Perot cavity inside which the radiating patch is placed as a primary feed. The EBG superstrate has the characteristic of PRS at the operating frequency of the antenna at which the magnitude of reflection coefficient is >0.55 and the reflection phase decreases linearly with frequency (see Fig. 8). Directivity of the primary antenna is enhanced due to multiple reflections of the radiating wave between the superstrate and the ground plane [13]. From the cavity, the wave is

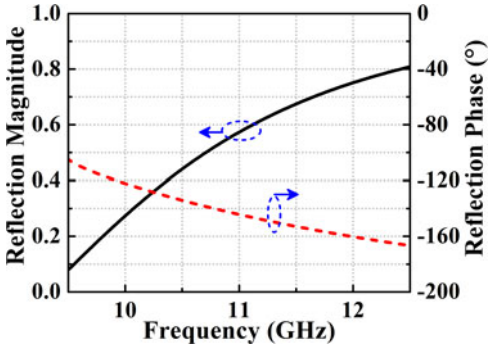


Fig. 8. Simulated reflection coefficient magnitude and phase variation of the proposed EBG superstrate.

https://doi.org/10.1017/S1759078721001768 Published online by Cambridge University Press

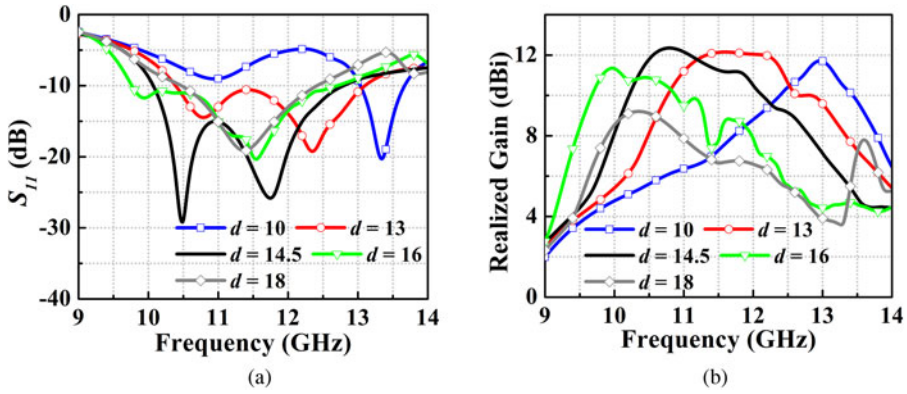


Fig. 9. Simulated (a) reflection coefficient and (b) gain variation of the proposed CRA at different air spacer heights.

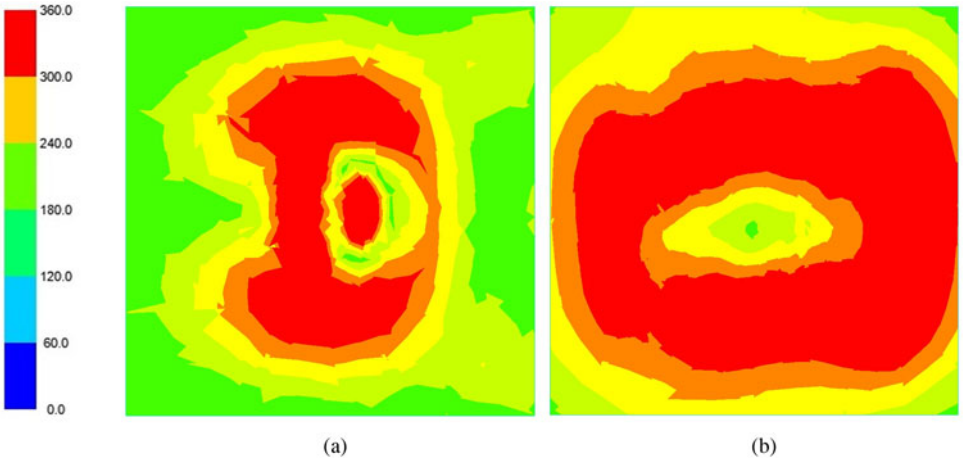


Fig. 10. Magnitude of tangential electric field distribution on a plane for (a) unloaded reference patch; (b) EBG superstrate-loaded cavity resonator antenna at frequency 11 GHz.

leaking out partially without any reflection while part of the wave is being transmitted after suffering reflection between the cavity walls. According to the principle of ray theory, two transmitted rays interfere constructively when the phase difference ($\Delta\phi$) between them is even multiple of 360° as obtained using (1) [13]

$$\Delta\phi = \phi_{PRS} - \pi - \frac{4\pi h'}{\lambda} = 2N\pi, \tag{1}$$

where $N = 0, 1, 2, \ldots$ (1)

Here ϕ_{PRS} is the reflection phase of the proposed EBG superstrate and "π" corresponds to change in phase after reflection from the PEC ground. Note that h' is the total height of the superstrate from the ground plane and this can be rearranged according to (2)

$$h' = d + 2h\sqrt{\varepsilon_r} = \left(\frac{\phi_{PRS}}{\pi} - 1\right)\frac{\lambda}{4} + N\frac{\lambda}{2}. \tag{2}$$

For the lowest order mode inside the cavity, N is equal to "0" and the height of the superstrate will be approximately $\lambda/2$ when the reflection phase of the superstrate is close to −180°. The gain and reflection coefficient of the proposed FP-CRA are illustrated in Fig. 7 along with the reference microstrip antenna. The performance of the proposed EBG as PRS is also compared with the dielectric superstrate-loaded RIS back antenna. Figure 7(b) shows the simulated peak realized gain of the combined antenna–superstrate structure reaches 12.35 dBi at 10.8 GHz with a gain improvement of 6.59 dB as compared with the reference antenna. Simulated impedance BW of the FPCA is 23.79% from 10.07 to 12.79 GHz and 3 dB gain BW is from 10.13 to 12.34 GHz (19.67%). The simulation result shows that composite antenna resonates at two frequencies center at 10.5 and 11.75 GHz. These two resonances correspond to radiating patch and the cavity resonance between the ground and PRS. EBG as PRS allows better impedance matching of the antenna over a wideband and a significant gain improvement as compared to dielectric superstrate. Sensitivities of the return loss and gain characteristics of the proposed FP-CRA are also observed by varying the superstrate height. Figures 9(a) and 9(b) present simulated S_{11} and the gain of the proposed antenna for different air spacer heights (d). Impedance matching and gain of this FP-CRA significantly depend on the height of the PRS. Finally, the optimum height is determined to be 14.5 mm through parametric variation in HFSS.

The improvement in gain due to superstrate loading can be explained by the electric field distribution over the radiating aperture of the FP-CRA. The unit cells of the EBG-superstrate behave as radiating elements due to partial reflecting characteristics and in effect increase the radiating aperture of the antenna.

https://doi.org/10.1017/S1759078721001768 Published online by Cambridge University Press

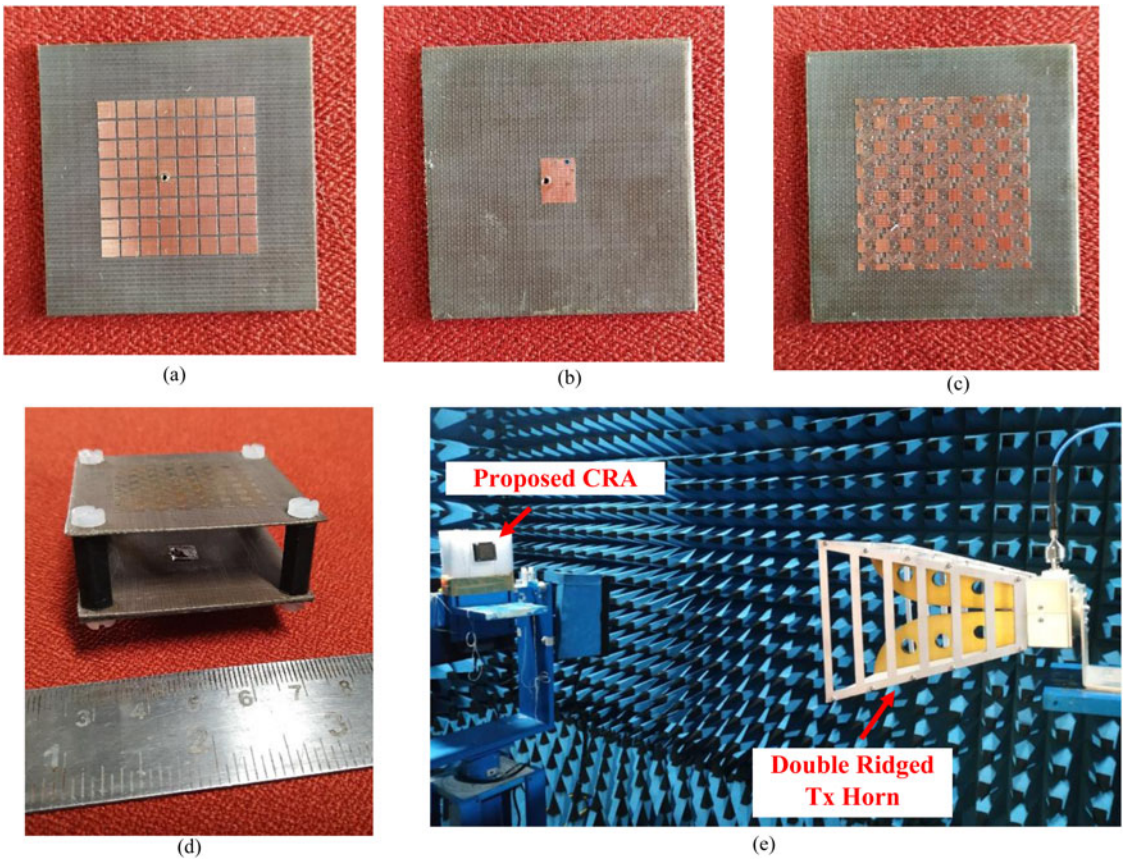


Fig. 11. Fabricated prototype of the proposed CRA (a) RIS; (b) rectangular patch; (c) EBG superstrate; (d) composite superstrate loaded antenna; (e) measurement setup inside the anechoic chamber.

Figure 10 shows the magnitudes of the tangential electric field on a plane at a distance of 2 mm away from the radiating patch for the unloaded reference antenna and that on a plane at 2 mm away from the EBG superstrate for the proposed FP-CRA. For the reference antenna, a significant variation of electric field magnitude exists over the radiating aperture, which causes the low gain of the primary feed antenna. When the patch antenna is loaded with the superstrate, a uniform field distribution is achieved over a large area which increases the radiating aperture of the antenna. The enhancement in the effective radiating aperture of the antenna causes a higher gain of the CRA. The field magnitude on the radiating aperture of the cavity antenna follows a Gaussian distribution. For superstrate with the infinite lateral size, the directivity enhancement of the CRA is related to the reflection magnitude (ρ) of the PRS using (3) [28]

$$D_r = 10\log\frac{1+\rho}{1-\rho}. \tag{3}$$

Figure 8 shows that at the resonance frequency of the primary feed antenna, the designed PRS has $\rho = 0.59$ which gives the calculated value of $D_r = 5.9$ dB. Thereby total directivity of CRA is obtained as $D = D_{feed} + D_r$. The directivity (D_{feed}) of the reference patch antenna is 7.7 dBi at the resonance and results in total directivity of the CRA as $D = 13.6$ dBi. Assuming 80% efficiency of the antenna, the aperture area (A) of the superstrate is determined using (4) [28]

$$A = \frac{10^{D/10}\lambda^2}{0.8\pi^2}. \tag{4}$$

Here λ is the wavelength at the operating frequency. The lateral size of the CRA is found as $1.7 \times 1.7\ \lambda^2$ for the required directivity of 13.6 dBi. The calculated radiating aperture size of the antenna closely matches with the actual aperture dimension of 45×45 mm^2 consisting of 49 FSS unit cells.

Experimental results

Figure 11 shows the photograph of the fabricated EBG superstrate-loaded CRA and the experimental setup inside an anechoic chamber to measure the radiation characteristics of the antenna. Four hexagonal nylon screws with a diameter of 5.8 mm are used to fix the superstrate layer at a height of 14.5 mm over the RIS-backed antenna. Measured reflection coefficients of without and with superstrate-loaded antenna are depicted in Fig. 12(a). In the absence of superstrate, antenna resonates at 10.79 GHz with 10 dB impedance BW of 10.26% (10.06–11.84 GHz). Measured $S_{11} < -10$ dB of the proposed FP-CRA with a single layer of EBG superstrate extends over 10.02–12.43 GHz (21.5%). The gain variation of the proposed antenna is shown in Fig. 12(b). Within the return loss BW, the peak gain of the RIS-backed primary feed antenna is 6.52 dBi at 10.8 GHz. After

https://doi.org/10.1017/S1759078721001768 Published online by Cambridge University Press

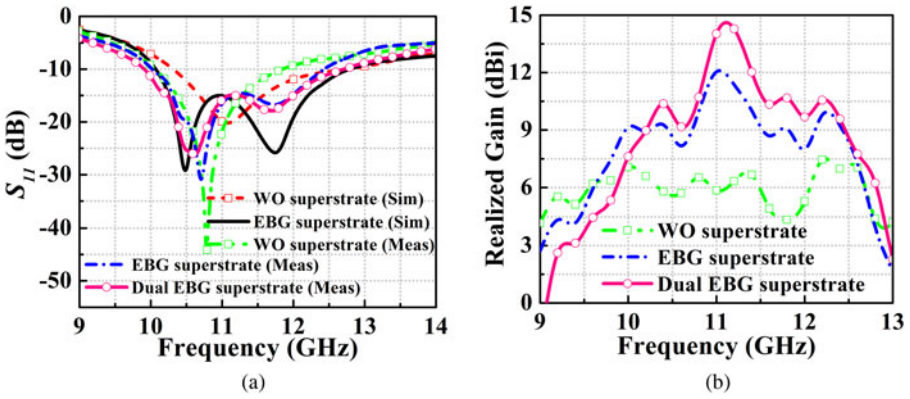


Fig. 12. Proposed CRA without and with superstrate loading: (a) simulated and measured reflection coefficient; (b) measured gain variation.

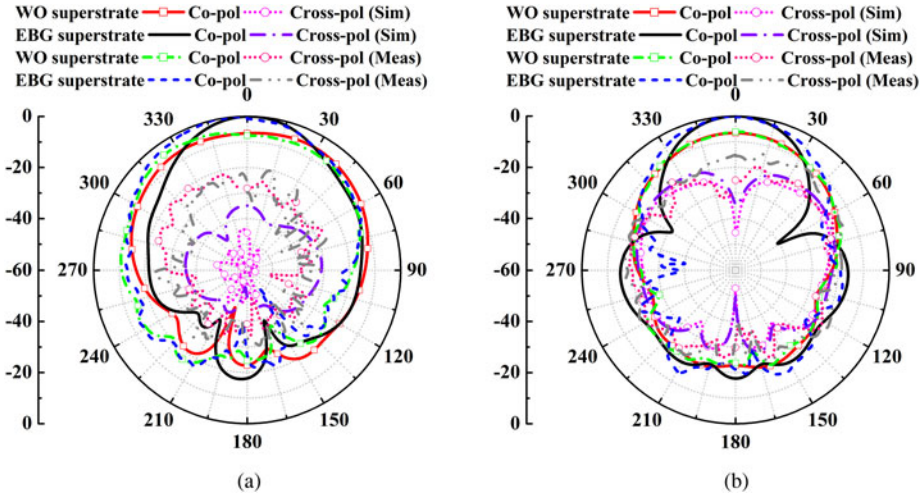


Fig. 13. Simulated and measured radiation patterns of the proposed CRA without and with superstrate loaded: (a) *E*-plane ($\varphi = 0°$); and (b) *H*-plane ($\varphi = 90°$).

EBG superstrate, loading peak gain is increased to 12.05 dBi with an improvement of 5.53 dB. The gain of the proposed antenna is further improved by using dual EBG superstrate layers. In measurement, spacing between the two EBG layers is optimized for maximum peak gain and the optimum value is obtained as 10.5 mm. Dual EBG superstrates stacking over the patch create two resonant cavities and cause an increase in BW. The measured impedance BW of the proposed dual EBG stacking FP-CRA is 9.91–12.71 GHz (24.8%) and having a peak gain of 14.3 dBi. The co-polarized and XPol radiation patterns of the proposed antenna are measured at the frequency 10.8 GHz. Figure 13 presents simulated and measured radiation patterns of the antenna in two principal planes (*E* and *H*) and both results are in good agreement with each other. A little discrepancy between simulated and measured patterns is noticed which can be attributed to the effects of the SMA connector and nylon spacer. Also, radiation losses from the cables bending and the variation in superstrate height can cause a mismatch in the patterns. The pattern shows a good co to XPol discrimination in both principal planes. Despite the measured XPol being a little higher as compared to simulated radiation patterns, the XPol is <-20 dB in *E*-plane and it is <-15 dB in *H*-plane. Patterns in both planes exhibit an increase in the directivity of the proposed CRA relative to the primary RIS-backed patch antenna.

Table 2 presents the performance comparison of the proposed FP-CRA with the previous works. The proposed antenna possesses higher BW as compared to [12, 19–22, 25, 27, 29]. The gain of the proposed CRA is more as compared to [23] and for the remaining works, the gain is comparable. The work in [24] has obtained higher BW and gain than the present work, but as a primary feed antenna open-ended waveguide is used in [24], which is bulky and increases the cost of the structure. The proposed work possesses the advantage of the miniaturized lateral dimension of only 1.62 λ_0 with a simple BW enhancement method of FP-CRA without any considerable compromise on the peak gain.

Antenna array with EBG superstrate

A 2×2 antenna array is printed over RIS-backed dielectric substrate as shown in Fig. 14. Here 12×12 RIS elements are used to cover the entire radiating aperture of the array. Each radiating patch of the array is uniformly excited using a microstrip line-based corporate feed network. Overall ground plane size of the array is 55 mm × 55 mm with patch dimension keeping same as those mentioned in the previous section. Center to center spacing between the array elements is 14.7 mm (0.525 λ_0 at 10.8 GHz) along both *x* and *y* axes. Figure 15 describes the simulated

https://doi.org/10.1017/S1759078721001768 Published online by Cambridge University Press

https://doi.org/10.1017/S1759078721001768 Published online by Cambridge University Press

Table 2. State-of-the-art performance comparison of the proposed broadband FP-CRA with previous works

Ref., year	Freq. (GHz)	Impedance BW $S_{11} < -10$ dB (%)	Peak gain (dBi)	3 dB Gain BW (%)	Lateral dimension (λ_0)	Profile (λ_0)	FTBR (dB)	XPol (dB)	No of superstrate	Superstrate type	Primary feed antenna
[12] 2016	10.8	~1.9%	14.39*	NA	1.98	0.58	16.2	NA	1	EBG	Microstrip feed patch
[19] 2016	13.9	5.24%	12.4	3.69%	2.27	0.25	14	NA	1	Slotted metal	AMC loaded probe feed patch
[20] 2019	7.45	8.69%	12.31	10.9%	1.89	0.64	10	10	2	Zero index metamaterial	Probe feed patch
[21] 2020	12.5	16.2%	12.89	12.5%	2.5	1.4	17	13	3	Meta-surface pol. converter	Aperture coupled patch
[22] 2015	5.82	4.92%	10.7	10.3%	1.75	0.6	15	NA	1	Meanderline metamaterial	Probe feed patch
[23] 2019	2.6	29.3%	9.95	29.3%	1.16	0.67	13	15	1	FSS	Differentially feed dielectric resonator antenna
[24] 2020	13	37%	14	32.3%	2.4	0.66	NA	NA	4	Multilayer complementary PRS	Waveguide feed
[25] 2012	12	3.52%	~12	NA	3.2	0.2	16	NA	1	Fishnet metasurface	AMC loaded probe feed patch
[26] 2019	5.85	28.6%	13.3	22.3%	2.44	0.45	20	15	1	Conventional square slot PRS	Probe feed with air dielectric patch
[27] 2019	13.8	12%	13.35	17.1%	2.67	0.65	NA	NA	2	Complementary FSS	Slot antenna
[29] 2018	7.7	12.38%	13.95	13%	1.54	0.96	15	15	2	Zero index metamaterial	RIS backed probe feed patch
This work	**10.8**	**21.5%**	**12.05**	**19.67%**	**1.62**	**0.61**	**22**	**15**	**1**	**EBG**	**RIS backed probe feed patch**
		24.8%	**14.3**	**15.9%**		**1**	–	–	**2**		

*Signifies simulated directivity.

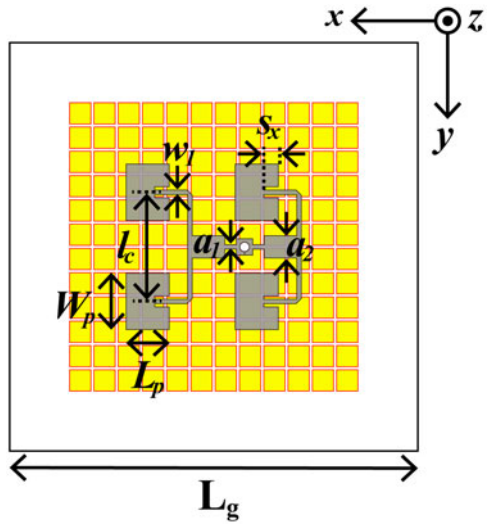


Fig. 14. Geometry of the 2 × 2 antenna array on the RIS. Design parameters are: $L_g = 55$, $L_p = 5.8$, $W_p = 7.6$, $a_1 = 0.6$, $a_2 = 3$, $w_1 = 0.6$, $l_c = 14.7$, $S_x = 1.95$. All units are in mm.

reflection coefficient and gain characteristics of this array without and with superstrate loading. For RIS-backed antenna array, the impedance BW for $S_{11} < -10$ dB extends from 10.13 to 11.81 GHz (15.3%). The peak gain of the proposed array without EBG superstrate is 11.7 dBi and it poses the advantage of gain variation <1.4 dB over the operating range. Further improvement in gain is obtained by placing an 8 × 8 EBG superstrate over the array elements at a distance of 14.5 mm from the patch surface. The proposed array fed FP-CRA shows reflection coefficient BW over 10.01–11.42 GHz (13.16%). Peak realized gain of the proposed CRA array is 13.45 dBi with the maximum gain variation over the operating frequency range being only 1.21 dB. The *E*- and *H*-plane radiation patterns of the antenna array without and with superstrate are shown in Fig. 16 at frequency 10.5 GHz. After loading the superstrate over the antenna array, the co-pol to XPol discrimination reduces due to scattering of the wave from the edges of PRS, still the XPol is <28 dB for both planes. The proposed array also exhibits a low SLL of 22.57 dB with 3 dB beamwidths in two principal planes are 38.4° and 33.7° respectively. FTBR of the proposed antenna array is 26.3 dB at 10.5 GHz. The gain of the proposed array can be further improved by increasing the superstrate lateral size >2.5 λ_0 or using multi stacking technique.

Conclusion

A novel uniplanar EBG unit is proposed in this paper having surface wave suppressing bandgap between 7.37 and 12.4 GHz (50.9%) which covers the entire X-band in the microwave spectrum. FSS characteristic of the proposed EBG is analyzed in detail by using it as a superstrate over a RIS-backed broadband patch antenna. RIS is used as an artificial ground for the patch to obtain impedance matching over a wide frequency range of operation. Measured results show that the proposed CRA has impedance BW of more than 20% with peak gain higher than 12 dBi.

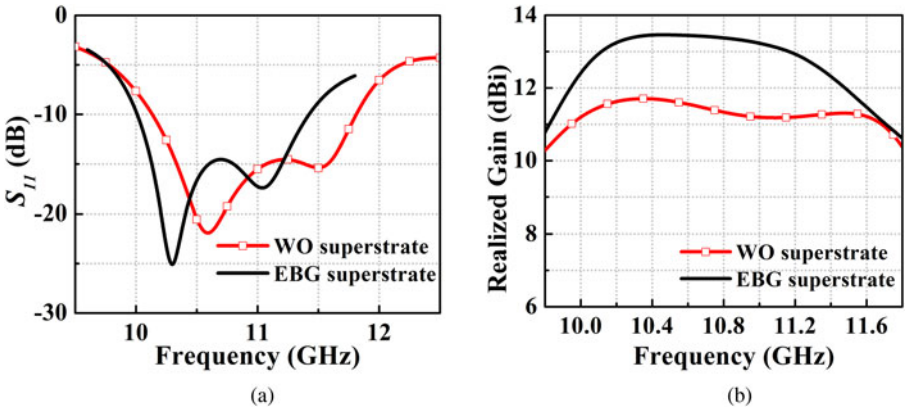


Fig. 15. Simulated (a) reflection coefficient and (b) gain variation of the proposed RIS-backed 2 × 2 antenna array without and with EBG superstrate loaded.

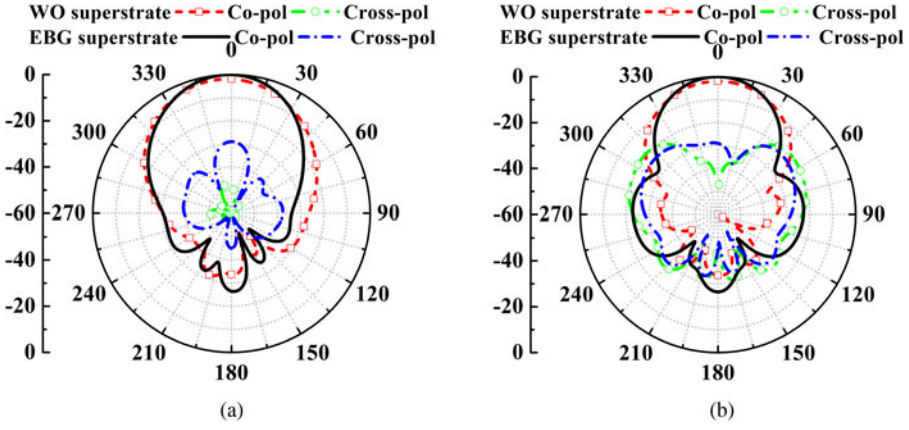


Fig. 16. Simulated radiation patterns of the proposed RIS-backed 2 × 2 antenna array without and with EBG superstrate loading: (a) *E*-plane; (b) *H*-plane.

https://doi.org/10.1017/S1759078721001768 Published online by Cambridge University Press

A flat gain over the operating BW is achieved by using a 2×2 antenna array as a primary feed of the proposed CRA. The gain variation below 1.21 dB with a maximum gain of 13.45 dBi has been obtained. The proposed broadband CRA has potential application for X-band radar and tracking systems. In future work, the proposed EBG will also be used as a decoupling network to improve the isolation between the antenna array.

Acknowledgement. The authors would like to express their profound gratitude to the Director of the Indian Institute of Technology Palakkad for setting up Central Instrumentational Facilities. This work is supported by the Science and Engineering Research Board, Government of India under project no: ECR/2018/002258. One of the authors thanks the support received from the Department of Science and Technology (DST), Government of India.

References

1. **Peddakrishna S, Khan T and De A** (2017) Electromagnetic band-gap structured printed antennas: a feature-oriented survey. *International Journal of RF and Microwave Computer-Aided Engineering* **27**, e21110.
2. **Sievenpiper D, Zhang L, Broas RFJ, Alexopolous NG and Yablonovitch E** (1999) High-impedance electromagnetic surfaces with a forbidden frequency band. *IEEE Transactions on Microwave Theory and Techniques* **47**, 2059–2074.
3. **Yang F-R, Ma K-P, Qian Y and Itoh T** (1999) A uniplanar compact photonic-bandgap (UC-PBG) structure and its applications for microwave circuit. *IEEE Transactions on Microwave Theory and Techniques* **47**, 1509–1514.
4. **Venkata SR and Kumari R** (2020) Gain and isolation enhancement of patch antenna using L-slotted mushroom electromagnetic bandgap. *International Journal of RF and Microwave Computer-Aided Engineering* **30**, e22369.
5. **Ashyap AYI, Abidin ZZ, Dahlan SH, Majid HA, Shah SM, Kamarudin MR and Alomainy A** (2017) Compact and low-profile textile EBG-based antenna for wearable medical applications. *IEEE Antennas and Wireless Propagation Letters* **16**, 2550–2553.
6. **Yang L, Fan M, Chen F, She J and Feng Z** (2005) A novel compact electromagnetic-bandgap (EBG) structure and its applications for microwave circuits. *IEEE Transactions on Microwave Theory and Techniques* **53**, 183–190.
7. **Coulombe M, Farzaneh Koodiani S and Caloz C** (2010) Compact elongated mushroom (EM)-EBG structure for enhancement of patch antenna array performances. *IEEE Transactions on Antennas and Propagation* **58**, 1076–1086.
8. **Bhavarthe PP, Rathod SS and Reddy KTV** (2017) A compact two via slot-type electromagnetic bandgap structure. *IEEE Microwave and Wireless Components Letters* **27**, 446–448.
9. **Kurra L, Abegaonkar MP, Basu A and Koul SK** (2013) A compact uniplanar EBG structure and its application in band-notched UWB filter. *International Journal of Microwave and Wireless Technologies* **5**, 491.
10. **Lin B-Q, Zheng Q-R and Yuan N-C** (2006) A novel planar PBG structure for size reduction. *IEEE Microwave and Wireless Components Letters* **16**, 269–271.
11. **Abedin MF, Azad MZ and Ali M** (2008) Wideband smaller unit-cell planar EBG structures and their application. *IEEE Transactions on Antennas and Propagation* **56**, 903–908.
12. **Kurra L, Abegaonkar MP, Basu A and Koul SK** (2016) FSS Properties of a uniplanar EBG and its application in directivity enhancement of a microstrip antenna. *IEEE Antennas and Wireless Propagation Letters* **15**, 1606–1609.
13. **Foroozesh A and Shafai L** (2010) Investigation into the effects of the patch-type FSS superstrate on the high-gain cavity resonance antenna design. *IEEE Transactions on Antennas and Propagation* **58**, 258–270.
14. **Yang W, Zhou J, Yu Z and Li L** (2014) Single-fed low profile broadband circularly polarized stacked patch antenna. *IEEE Transactions on Antennas and Propagation* **62**, 5406–5410.
15. **Deshmukh A and Ray KP** (2015) Analysis of broadband variations of U-slot cut rectangular microstrip antennas. *IEEE Antennas and Propagation Magazine* **57**, 181–193.
16. **Ray K, Sevani V and Kakatkar S** (2006) Compact broadband gap-coupled rectangular microstrip antennas. *Microwave and Optical Technology Letters* **48**, 2384–2389.
17. **Liu W, Chen ZN and Qing X** (2014) Metamaterial-based low-profile broadband mushroom antenna. *IEEE Transactions on Antennas and Propagation* **62**, 1165–1172.
18. **Meng F, Liu Y and Sharma SK** (2020) A miniaturized patch antenna with enhanced bandwidth by using reactive impedance surface ground and coplanar parasitic patches. *International Journal of RF and Microwave Computer-Aided Engineering* **30**, e22225.
19. **Liu Z, Cao Z and Wu L** (2016) Compact low-profile circularly polarized Fabry–Perot resonator antenna fed by linearly polarized microstrip patch. *IEEE Antennas and Wireless Propagation Letters* **15**, 524–527.
20. **Rajanna PKT, Rudramuni K and Kandasamy K** (2019) A high-gain circularly polarized antenna using zero-index metamaterial. *IEEE Antennas and Wireless Propagation Letters* **18**, 1129–1133.
21. **Huang R, Wang Z, Li G, Lin C, Ge Y and Pu J** (2020) A metasurface enabled wideband high-gain dual-circularly-polarized Fabry-Perot resonator antenna. *Microwave and Optical Technology Letters* **62**, 3195–3202.
22. **Razi ZM, Rezaei P and Valizade A** (2015) A novel design of Fabry-Perot antenna using metamaterial superstrate for gain and bandwidth enhancement. *AEÜ – International Journal of Electronics and Communications* **69**, 1525–1532.
23. **Gupta RD and Parihar MS** (2019) Differentially driven wideband Fabry–Perot cavity antenna. *IET Microwaves, Antennas & Propagation* **13**, 2365–2371.
24. **Niaz MW, Yin Y, Bhatti RA, Cai Y-M and Chen J** (2021) Wideband Fabry–Perot resonator antenna employing multilayer partially reflective surface. *IEEE Transactions on Antennas and Propagation* **69**, 2404–2409. doi: 10.1109/TAP.2020.3022555.
25. **Li L, Lei S and Liang C-H** (2012) Metamaterial-based Fabry–Perot resonator for ultra-low profile high-gain antenna. *Microwave and Optical Technology Letters* **54**, 2620–2623.
26. **Ta SX, Nguyen TH-Y, Nguyen KK and Dao-Ngoc C** (2019) Bandwidth enhancement of circularly-polarized Fabry-Perot antenna using single layer partially reflective surface. *International Journal of RF and Microwave Computer-Aided Engineering* **29**, e21774.
27. **Meriche MA, Attia H, Messai A, Mitu SSI and Denidni TA** (2019) Directive wideband cavity antenna with single-layer meta-superstrate. *IEEE Antennas and Wireless Propagation Letters* **18**, 1771–1774.
28. **Wang N, Liu Q, Wu C, Talbi L, Zeng Q and Xu J** (2014) Wideband Fabry-Perot resonator antenna with two complementary FSS layers. *IEEE Transactions on Antennas and Propagation* **62**, 2463–2471.
29. **Majumder B, Kandasamy K and Ray KP** (2018) A zero index based meta-lens loaded wideband directive antenna combined with reactive impedance surface. *IEEE Access* **6**, 28 746–28 754.



Soumik Dey (student member, IEEE) graduated in physics (Hons.) from Ramakrishna Mission Residential College, Narendrapur in 2012. He received B.Tech. and M.Tech. in radio physics and electronics from the University of Calcutta in 2016 and 2018, respectively. He is currently pursuing a Ph.D. degree at the Department of Electrical Engineering, Indian Institute of Technology Palakkad, India. From December 2018 to June 2019, he worked as a research staff at IIT Palakkad where he joined the Ph.D. program in July 2019. He has published more than 10 research papers and filed two patents. His current research interest includes frequency selective surface, electromagnetic bandgap structure, multiband and broadband microstrip antenna, and substrate integrated waveguide. He is also a recipient of the DST Inspire Fellowship from the Government of India.

https://doi.org/10.1017/S1759078721001768 Published online by Cambridge University Press



Sukomal Dey (senior member, IEEE) received B.Tech degree in electronics and communication engineering at the West Bengal University of Technology, Kolkata, India, in 2006, an M.Tech in mechatronics engineering at the Indian Institute of Engineering Science and Technology (IIEST), Shibpur, India, and obtained an M.Tech in one year from the Central Electronics Engineering Research Institute (CEERI-CSIR), Pilani, India, in 2009. Dr. Dey obtained a Ph.D. from the Centre for Applied Research in Electronics (CARE), Indian Institute of Technology Delhi in July 2015. From August 2015 to July 2016 he was working as a project scientist in the Industrial Research and Development (IRD) centre, IIT Delhi. He also worked on a collaborative research project supported by Synergy Microwave Corp., NJ, USA during the same period. From August 2016 to June 2018, he was working in the Radio Frequency Microsystem Lab (RFML), National Tsing Hua University, Taiwan, as a postdoctorate research fellow. Since June 2018 he is working as an assistant professor at the Department of Electrical Engineering, Indian Institute of Technology Palakkad, Kerala.

Dr. Dey is a recipient of the Postgraduate Student Award from the Institute of Smart Structure and System, Bangalore, in 2012, Best Industry Relevant Ph.D. Thesis Award from the Foundation for Innovation in Technology Transfer, IIT Delhi in 2016, Postdoctoral Fellow Scholarships from the Ministry of Science and Technology (MOST), Taiwan in 2016 and 2017, respectively, Early Career Research Award (ECRA) from the Science and Engineering Research Board (SERB), Government of India in 2019 and Smt. Ranjana Pal Memorial Award (2021) from the Institution of Electronics and Communication Engineers (IETE). He has authored/co-authored more than 70 research papers, one state-of-the art book, and two book chapters. Dr. Dey holds three and filed six patents. His research interests include: RF MEMS, microwave, to sub-mm wave metamaterial structures and microwave integrated circuits including antennas.

https://doi.org/10.1017/S1759078721001768 Published online by Cambridge University Press